In-situ Doppler-free spectroscopy and laser frequency stabilization based on time-division multiplexing differential saturated absorption

Yuxin Wang[†,1,2] Zhiyue Zheng[†,2] Qiuxin Zhang,[1,2] Yonglang Lai,[1,2] Zongqi Ge,[1,2] Tianyi Wang,[1,2] Liangyu Ding,[2] Smirnov Vasilii,[3,4] Shuaining Zhang,[1,2,5] Wei Zhang,[1,2,5] and Xiang Zhang[1,2,5]

[1)] *Department of Physics and Beijing Key Laboratory of Opto-electronic Functional Materials and Micro-nano Devices, Renmin University of China, 100872 Beijing, China*

[2)] *Beijing Academy of Quantum Information Sciences, 100193 Beijing, China*

[3)] *P.N. Lebedev Physical Institute of the Russian Academy of Sciences, Moscow 119991, Russia*

[4)] *Russian Quantum Center, Skolkovo, Moscow 121205, Russia*

[5)] *Key Laboratory of Quantum State Construction and Manipulation (Ministry of Education), Renmin University of China, 100872 Beijing, China*

(*Electronic mail: siang.zhang@ruc.edu.cn)

(Dated: 24 April 2024)

We introduce a novel time-division multiplexing differential saturated absorption spectroscopy (TDMDSAS) approach, providing superior accuracy and stability in Doppler-free spectroscopy. By distinguishing probe and reference fields in the temporal domain, TDMDSAS efficiently suppresses Doppler broadening and common-mode optical noise. We utilized this technology to determine the absolute frequency of diverse neutral Yb isotopes across its $6s^2\ ^1S_0 \rightarrow 6s6p^1P_1$ transitions. Furthermore, the first-ever observation of in-situ Doppler-free Zeeman sub-level spectra was accomplished, enabling the determination of magnetic field gradients. We stabilized a UV diode laser at 399nm by utilizing the error signal derived from the time-differential spectral signal of ^{174}Yb. This technique yielded a frequency instability of 15 kHz with a 40 s averaging time and a standard deviation of around 180 kHz over a half-hour period. Given its low cost, straightforward, and scalable nature, TDMDSAS holds excellent potential in metrology and quantum applications.

So far, a variety of techniques for spectroscopy and laser frequency stabilization have been developed in laboratory setting, encompassing saturated absorption spectroscopy (SAS)[1–4], modulation transfer spectroscopy (MTS)[5–8], dichroic atomic vapor laser lock (DAVLL)[9–11], polarization spectroscopy (PS)[12,13], scanning transfer cavity lock (STCL)[14,15], and Pound-Drever-Hall (PDH) frequency-locking[16,17]. Among them, SAS is a well-established and extensively utilized technique for high-resolution spectroscopy and laser frequency stabilization.

In the standard SAS scheme, only the Voigt profile is captured, necessitating an additional reference field to obtain a Doppler-free spectrum. This exacerbates system's complexity and makes it susceptible to inhomogeneous background absorption. MTS involves a high-frequency modulation of the pump beam that reduces susceptibility to the Doppler background and directly obtains a dispersion-like signal using two beams. Regrettably, the optical modulator could produce residual amplitude modulation (RAM) to the optical field[18,19], potentially distorting the dispersed-like signal. Similarly, PS exclusively acquires the dispersion-like lineshape and is profoundly impacted by the optical polarization purity, despite without any modulation. The single-beam SAS[20,21] enhances SAS by utilizing the space-division multiplexing method but it still contends with issues of structural stability. Additionally, it is incapable of measuring the magnetic field gradient due to the opposite orientation of the "two probe beams".

To overcome these limitations, we introduce a more straightforward, efficient, and cost-effective technique: time-division multiplexing differential saturated absorption spectroscopy (TDMDSAS). This approach transforms spatially separated probe and reference beams into temporally distinct entities, thereby enabling memory-based digital signal processing[22,23]. Our method simultaneously captures high-resolution, noise-suppressed in-situ Doppler-free signals, together with demodulated signals for laser frequency stabilization. We measure the absolute frequency of the $6s^2\ ^1S_0 \rightarrow 6s6p\ ^1P_1$ transition in Yb isotopes, the frequency shifts of Zeeman sub-levels under different magnetic field strengths, and perform frequency stabilization on the 399nm laser. The laser is stabilized to the transition of ^{174}Yb at 751526399.672 MHz, achieving frequency instability of 15 kHz with an averaging time of 40 s, and a standard deviations of roughly 180 kHz over 2000 s. Moreover, our method features the proficiency to detect magnetic field gradients. This innovative method holds immense potential for extension to other atomic species and offers practical significance for applications in atomic clocks[24], atomic magnetometers[25] and quantum computation[26,27].

The experimental setup is shown in Fig.1. A 399nm ultraviolet diode laser (DLC DL PRO HP) is directed through two polarization beam splitters (PBS), partitioning its output into three distinct beams. One of the beams is directed towards a wavelength meter (HighFinesse WS-8, WLM) for frequency measurement. The remaining two beams serve as the probe beam and the pump beam, both of which are tightly focused through a lens into a hollow cathode lamp (Hamamatsu L2783, HCL). To achieve a Doppler-free spectrum with an optimal signal-to-noise ratio, we finely tuned the power and polarization using PBS and half-wave plates (HWP) and optimized the operating current of the Yb HCL. Upon finalizing these parameters, the HCL's driving voltage was set at 197 V with a stable current of 1.3 mA. Directly before entering the HCL, the intensity of the probe beam was maintained at

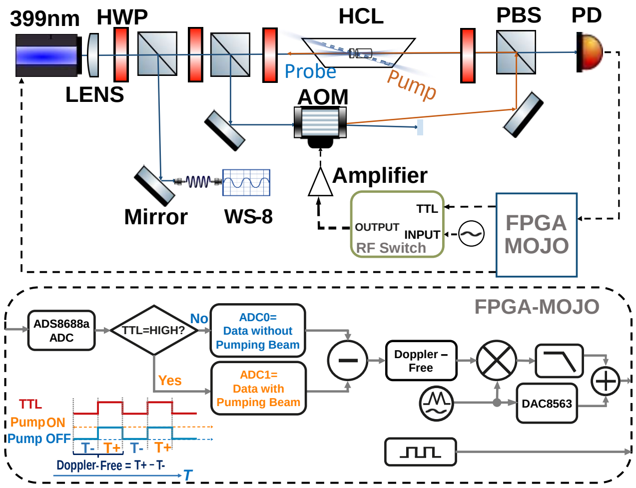

FIG. 1. (Color online) Schematic diagram of the experimental setup: half-wave plate (HWP), polarization beam splitter (PBS), hollow cathode lamp (HCL), acousto-optic modulator (AOM), photodetector (PD), wavelength meter(WS-8). The dashed box at the bottom illustrates the process of internal signal digitized processing within the FPGA.

200 μW, and that of the pump beam at 500 μW. Within the atomic sample, the waists of the probe beam and pump beam were approximately 450 μm. The precise alignment of the probe beam with the counter-propagating pump beam is crucial to avoid RAM[5,18,28,29], which could distort the signal. After traversing through the HCL, the probe beam is detected by a photodetector (PDA100A, PD) with a 40 dB gain. The acquired signal is then parsed by an analog-to-digital converter (ADC) and subsequently analyzed by an FPGA.

To ensure a pristine Doppler-free signal without any distortion, we utilized the concept of time-interleaved ADC, which interleaves sampling of the same signal over time and maintaining a shared sampling rate, thereby allowing for high-speed data acquisition without distinctly sacrificing signal integrity. In our setup, the pump beam's frequency is shifted by 200 MHz using an acousto-optic modulator (SGT200-397-1TA, AOM)[30], which is controlled by a TTL signal from the FPGA through an RF switch. The high and low states of the TTL signal determine the presence or absence of the pump beam, and the switching frequency can reach up to 50 MHz. However, due to the response time constraints of the atoms, PD, AOM, and potential interleaving spurs in signal processing, we opted for a TTL signal frequency of 20 kHz. After receiving the detection beam signal from the PD, the FPGA performs time-domain differentiation, based on the state of the TTL signal, to retrieve Doppler-free signals. The two signals of difference originate from the same probe beam, enabling the acquisition of in-situ Doppler background information within the pump-probe region for the identical atoms group. Consequently, the resulting Doppler-free signal exhibits exceptional robustness. To generate the error signal for laser frequency stabilization, a 47 kHz sine wave modulation signal is applied to the diode voltage of the laser. If modulation is applied solely to the pump beam via AOM, it results in amplitude modulation and necessitates a higher modulation frequency and depth to achieve MTS. We derive the error signal by mixing the Doppler-free signal with the modulation signal and processing it through a digital lock-in amplifier. The error signal is then processed by the proportional-integral-differential (PID) controller and fed back to the laser controller for frequency stabilization. The controller board, incorporating FPGA (Spartan6 LX9), DAC (DAC8563), and ADC (ADS8688A), integrates multiple functions including time-domain signal processing, digital lock-in amplifier, digital PID controller, digital filter, and digital signal generation. Moreover, the controller board and highly engineered interactive software remarkably assist in acquiring Doppler-free spectra and laser frequency stabilization.

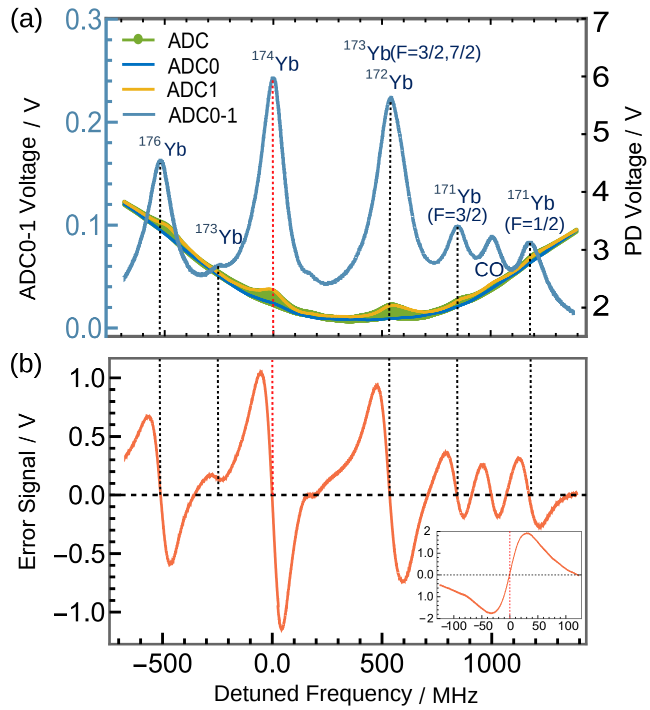

FIG. 2. (Color online) (a) The spectrum of ${}^{1}S_{0} \rightarrow {}^{1}P_{1}$ transition of Yb, V_{ADC}(green, dots) represents all the signals received from the PD, V_{ADC0} (blue, solid), indicative of Doppler- broadened absorption while the TTL is in a low state, V_{ADC1}(yellow, solid) corresponds to saturated absorption peaks with a high TTL signal, and the Doppler-free spectrum $V_{\mathrm{ADC0-1}}$ (light blue, solid) is obtained by differencing V_{ADC0} from V_{ADC1}. (b) The associated first-derivative demodulation signal is derived from $V_{\mathrm{ADC0-1}}$. The inset shows a detailed image of the demodulation signal of ^{174}Yb for laser frequency stabilization. The detunings are relative to the absolute frequency of the ^{174}Yb transition.

The typical SAS signal can be described with a Voigt profile, representing the superposition of two lineshapes[20]: the Doppler broadening with a Gaussian profile and the natural linewidth with a Lorentzian profile

$$D(\omega,\omega_0) = \frac{2\sqrt{\ln 2}}{\sqrt{\pi}\Gamma} \exp\left[\frac{-2\sqrt{\ln 2}(\omega-\omega_0)^2}{\Gamma}\right] \quad (1)$$

$$S(\omega) = \frac{\gamma/2\pi}{(\omega-\omega_0)^2+(\gamma/2)^2} + D(\omega,\omega_0) \quad (2)$$

where ω is the laser frequency and ω_0 is the atomic transition frequency. γ and Γ represent the full width at half maximum (FWHM) of the Lorentzian and Gaussian line shapes, respectively. To acquire the error signal sent to the feedback loop for frequency stabilization, we apply a modulation signal $A\sin(\Omega t)$ set an operating point for demodulating the signal with the first harmonic, culminating in the following result,

$$\begin{aligned}&\frac{1}{T}\int_0^T \sin(\Omega t) S[\omega_0 + A\sin(\Omega t)] \\ &= \frac{A}{2}\left\{\frac{-\gamma(\omega-\omega_0)}{\pi[(\omega-\omega_0)^2+(\gamma/2)^2]^2} + D^{(1)}(\omega,\omega_0)\right\}\Bigg|_{\omega}\end{aligned} \quad (3)$$

where $T = 2\pi/\Omega$ and $D^{(1)}(\omega,\omega_0)$ is the first derivative of $D(\omega,\omega_0)$, and A is the modulation depth. During the demodulation process, we scan ω to generate a dispersive-like lineshape. We aim to mitigate the Doppler background as effectively as possible to achieve a superior Doppler-free spectrum.

Pulse amplitude modulation is applied to the pump beam in the TDMDSAS setup. A low TTL signal indicates the absence of the pump beam, inducing a significant broadening of the atomic absorption spectrum due to the Doppler effect. This broadening results in the Doppler broadening profile as described in Eq.1. A high TTL signal denotes the presence of the pump laser, due to different velocity groups in resonance with each beam. The higher-power pump beam effectively contributes to saturated absorption fatigue for the probe field, yielding the characteristic profile of SAS as described in Eq.2. The received signal undergoes automatic and real-time difference to generate the Doppler-free signal $S(\omega) - D(\omega)$ as the TTL signal alternates between its states. Specifically, the FPGA processes the received signal, V_{ADC}, from the PD into three categories based on the TTL signal's states. As indicated in Fig.2(a), these include the Doppler-broadened absorption signal V_{ADC0}, the saturated absorption signal V_{ADC1}, and the Doppler-free signal $V_{\mathrm{ADC0-1}}$. Furthermore, Fig.2(b) displays the spectral first-derivative demodulated signal of the $V_{\mathrm{ADC0-1}}$, as explained in the first term on the right side of Eq.3.

In the TDMDSAS scheme, we can extract in-situ Doppler background information, including orientation. This capability contributes to Doppler-free spectra exhibiting exceptional long-term absolute stability and enhanced resolution, outperforming alternative differential schemes. The frequency shifts of the transitions for different isotopes of Yb relative to the transition frequency in ^{174}Yb are presented in Table I. The absolute frequency of ^{174}Yb is determined to be 751526399.672 ± 2.3 MHz. The deviation in absolute frequency from other results primarily originates from variations in the pumping AOM's operating frequencies, leading to different frequency shifts between the probe and pump fields[4]. During our ten daily measurements, the standard deviation remained consistently within 2.3 MHz, mainly due to varying operational conditions of the WLM unit, which also contributes to the difference between our results and absolute frequency readings from Ref[6].

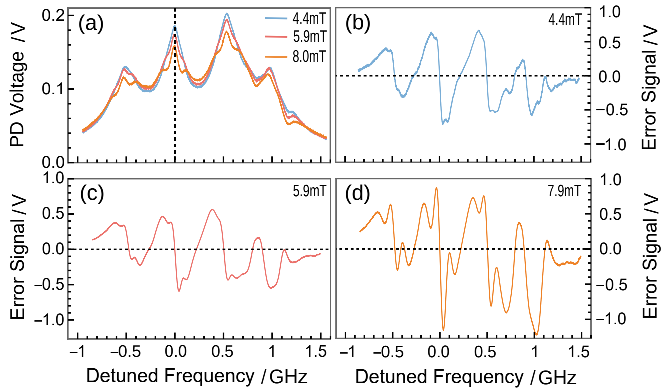

FIG. 3. (Color online) (a) The TDMDSAS are observed under magnetic field strengths of 4.4, 5.9, and 7.9 mT. (b,c,d) Corresponding first-derivative demodulated signals of three different magnetic fields. The detunings are relative to the absolute frequency of the ^{174}Yb transition.

The spectroscopy linewidth of the $^1S_0 \rightarrow ^1P_1$ transition in ^{174}Yb measured by our approach, is approximately 65 MHz, broader than the natural linewidth of 29 MHz, reaching the minimum SAS resolution[6]. The broadening observed in the Doppler-free signal is believed to be attributed to collisional dephasing, induced by the buffer gas (Ne) sealed in the HCL[31,32]. To further ensure the minimum resolution of TDMDSAS, we applied external magnetic fields aligned parallel to the probe beam using the permanent magnet. This setup permitted the observation of Doppler-free spectra featuring Zeeman sub-levels and the absolute Zeeman splitting frequency more accurately. The magnetic field intensity is adjusted by altering the placement of the permanent magnet, and it is important to note that the magnetic shielding effect of the hollow cathode should be considered[9,10]. As illustrated in Fig.3, we investigated the Doppler-free spectroscopy under diverse magnetic field strengths at 4.4, 5.9, and 7.9 mT, corresponding Zeeman sub-level shifts are 64, 85, and 115 MHz. Table I shows the frequency shifts of ^{176}Yb, ^{174}Yb, and ^{172}Yb under a magnetic field of 7.9 mT. As observed from Fig.3(b), when the magnetic field reaches 4.4 mT, it is evident that the Zeeman splitting at a frequency of 64 MHz is still distinguishable. The resolution has reached its optimum limits due to the constraints imposed by the FWHM of the peaks. However, as the magnetic field intensifies, the Zee-

TABLE I. **Measured absolute frequencies of $^1S_0 \rightarrow ^1P_1$ transition and frequency shifts relative to ^{174}Yb**

Isotope	Shifts (MHz)	$m=1$	$m=-1$
^{176}Yb	-508.66	-394	-623
^{173}Yb($F=5/2$)	-239.26	-	-
^{174}Yb	0	114	-116
^{172}Yb	538.81	654	424
^{171}Yb($F=3/2$)	840.24	-	-
^{171}Yb($F=1/2$)	1173.70	-	-

man sub-levels of ^{171}Yb risk being submerged into neighboring peaks. Our method, engineered for precision measurement of both the magnetic field and its gradient, effectively navigates around hurdles inherent in conventional SAS techniques, wherein magnetic field disparities originate due to the spatial separation between the probe and reference beams.

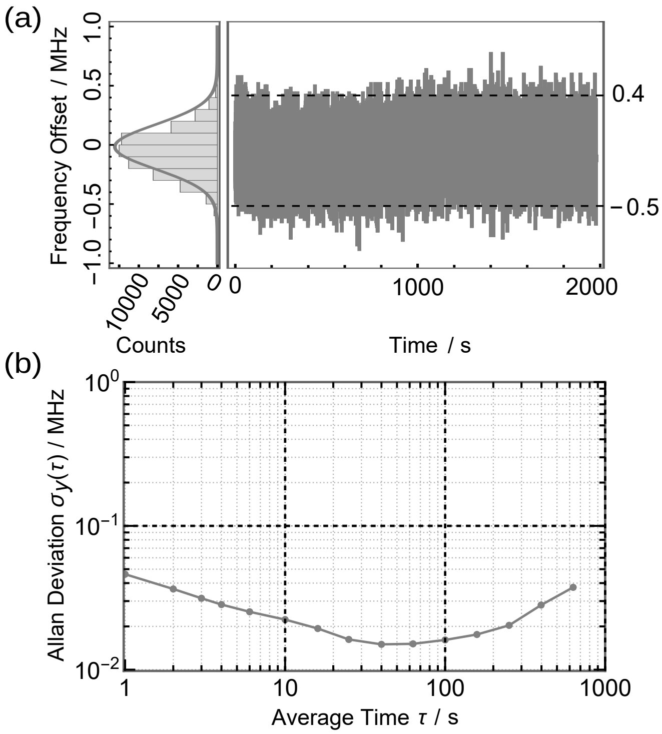

FIG. 4. (a) The frequency drift when the laser is locked to the ^{174}Yb transition using our method. The Gaussian histogram depicts the distribution of frequency offsets relative to the central frequencies. (b) Allan deviation $\sigma_y(\tau)$ of the frequency fluctuation is plotted as a function of average time when the laser is stabilized to the $^1S_0 \rightarrow ^1P_1$ transition in ^{174}Yb, measured by the WLM using our refined method.

To quantify the frequency stability and achieve optimal laser frequency stabilization, we meticulously locked the laser at the zero-crossing point of the dispersion signal corresponding to the transitions of ^{174}Yb ($^1S_0 \rightarrow ^1P_1$), as indicated in the inset of Fig.2(b). This process stabilized the target laser at a wavelength of 398.911413 nm over an extended period. Fig.4(a) illustrates the drift measurements of the laser when it is locked using our method, revealing a frequency standard deviation of 180 kHz. The histogram on the left side depicts the deviations in the laser frequency from its central frequency, with FWHM of 0.44 MHz. Overall measurements span over 2000 s, and we are interested in calculating the Allan deviation $\sigma_y(\tau)$ of the frequency fluctuation measured by the WLM. Initially, it was at 46 kHz when $\tau = 1$ s, and decreased to 15 kHz when $\tau = 40$ s. However, it eventually increased to 37 kHz when $\tau = 1000$ s, as shown in Fig.4(b). This behavior could arise from long-term drifts in the WLM itself[33].

In summary, a straightforward, versatile, and efficient TD-MDSAS method has been innovatively established. Given the capability to capture in-situ Doppler background information including direction, this scheme exhibits excellent noise suppression on the Doppler-free spectrum. Our efforts encompass absolute frequency measurements of Yb isotopes, exploration of Doppler-free spectra with Zeeman levels, and the achievement of high-performance laser frequency stabilization. Furthermore, the in-situ magnetic field measurement functionality broadens its application potential for magnetic field gradient determination. This protocol widely applies to laser cooling experiments and can be extended to various types of lasers and atomic species. It presents significant implications for atoms and ions quantum computation and practical value in applications such as atomic clocks, atomic magnetometers, and atomic interferometers.

The authors acknowledge financial support from the National Natural Science Foundation of China (12074427, 12074428, 12204535, 12304565, 92265208) and the National Key R&D Program of China (2022YFA1405300).

REFERENCES

[1] Ayan Banerjee and Vasant Natarajan. Saturated-absorption spectroscopy: eliminating crossover resonances by use of copropagating beams. *Optics Letters*, 28(20):1912, October 2003.

[2] Paul Burdekin, Samuele Grandi, Rielly Newbold, Rowan A. Hoggarth, Kyle D. Major, and Alex S. Clark. Single-photon-level sub-doppler pump-probe spectroscopy of rubidium. *Phys. Rev. Appl.*, 14:044046, Oct 2020.

[3] Moustafa Abdel Hafiz, Grégoire Coget, Emeric De Clercq, and Rodolphe Boudot. Doppler-free spectroscopy on the Cs D1 line with a dual-frequency laser. *Opt. Lett.*, 41(13):2982–2985, July 2016.

[4] Pengyuan Chang, Duo Pan, Haosen Shang, Tiantian Shi, and Jingbiao Chen. A global crossover saturated-absorption spectroscopy induced by dual-frequency laser. *Journal of Physics B: Atomic, Molecular and Optical Physics*, 53(20):205402, October 2020.

[5] Dali Sun, Chao Zhou, Lin Zhou, Jin Wang, and Mingsheng Zhan. Modulation transfer spectroscopy in a lithium atomic vapor cell. *Optics Express*, 24(10):10649, May 2016.

[6] Takehiko Tanabe, Daisuke Akamatsu, Hajime Inaba, Sho Okubo, Takumi Kobayashi, Masami Yasuda, Kazumoto Hosaka, and Feng-Lei Hong. A frequency-stabilized light source at 399 nm using an Yb hollow-cathode lamp. *Japanese Journal of Applied Physics*, 57(6):062501, June 2018.

[7] Min Zhou, Sheng Zhang, Limeng Luo, and Xinye Xu. Characterization of ytterbium resonance lines at 649 nm with modulation-transfer spectroscopy. *Physical Review A*, 101(6):062506, June 2020.

[8] Hao Qiao, Luhua Liu, Min Zhou, Limeng Luo, and Xinye Xu. Investigation of the $6s6p\ ^3p_2$ - $6s7s\ ^3s_1$ transition of ytterbium atoms with modulation-transfer spectroscopy. *Applied Physics Letters*, 122(22):224002, May 2023.

[9] Takumi Sato, Yusuke Hayakawa, Naohiro Okamoto, Yusuke Shimomura, Takatoshi Aoki, and Yoshio Torii. Birefringent atomic vapor laser lock in a hollow cathode lamp. *JOSA B*, 39(1):155–159, January 2022.

[10] Jae Ihn Kim, Chang Yong Park, Jin Yong Yeom, Eok Bong Kim, and Tai Hyun Yoon. Frequency-stabilized high-power violet laser diode with an ytterbium hollow-cathode lamp. *Optics Letters*, 28(4):245–247, February 2003.

[11] E.D. van Ooijen, G. Katgert, and P. van der Straten. Laser frequency stabilization using Doppler-free bichromatic spectroscopy. *Applied Physics B*, 79(1):57–59, July 2004.

[12] Shaobing Zhu, Tao Chen, Xiaolin Li, and Yuzhu Wang. Polarization spectroscopy of $^1s_0 - ^1p_1$ transition of neutral ytterbium isotopes in hollow cathode lamp. *J. Opt. Soc. Am. B*, 31(10):2302–2309, Oct 2014.

[13] Michael W. Lee, Marie Claire Jarratt, Christian Marciniak, and Michael J. Biercuk. Frequency stabilization of a 369 nm diode laser by nonlinear spectroscopy of Ytterbium ions in a discharge. *Optics Express*, 22(6):7210–7221, March 2014.

[14] Shira Jackson, Hiromitsu Sawaoka, Nishant Bhatt, Shreyas Potnis, and Amar C. Vutha. Laser frequency stabilization using a transfer interferometer. *Review of Scientific Instruments*, 89(3):033109, March 2018.

[15] S. Subhankar, A. Restelli, Y. Wang, S. L. Rolston, and J. V. Porto. Microcontroller based scanning transfer cavity lock for long-term laser frequency stabilization. *Review of Scientific Instruments*, 90(4):043115, April 2019.

[16] Yong Zeng, Zhuo Fu, Yang-Yang Liu, Xiao-Dong He, Min Liu, Peng Xu, Xiao-Hong Sun, and Jin Wang. Stabilizing a laser frequency by the Pound–Drever–Hall technique with an acousto-optic modulator. *Applied Optics*, 60(5):1159–1163, February 2021.

[17] Xiao Wang, Lishuang Feng, Jun Xu, and Peiren Ni. Steady-state frequency-tracking distortion in the digital Pound–Drever–Hall technique. *Applied Optics*, 59(5):1347–1352, February 2020.

[18] Esa Jaatinen and David J. Hopper. Compensating for frequency shifts in modulation transfer spectroscopy caused by residual amplitude modulation. *Optics and Lasers in Engineering*, 46(1):69–74, January 2008.

[19] V. Negnevitsky and L. D. Turner. Wideband laser locking to an atomic reference with modulation transfer spectroscopy. *Optics Express*, 21(3):3103, February 2013.

[20] Bowen Wang, Xiang Peng, Haidong Wang, Yang Liu, and Hong Guo. Laser-frequency stabilization with differential single-beam saturated absorption spectroscopy of 4he atoms. *Review of Scientific Instruments*, 93(4):043001, April 2022.

[21] A. Sargsyan, A. Amiryan, Y. Pashayan-Leroy, C. Leroy, A. Papoyan, and D. Sarkisyan. Approach to quantitative spectroscopy of atomic vapor in optical nanocells. *Opt. Lett.*, 44(22):5533–5536, November 2019.

[22] M. Carminati and G. Scandurra. Impact and trends in embedding field programmable gate arrays and microcontrollers in scientific instrumentation. *Review of Scientific Instruments*, 92(9):091501, September 2021.

[23] Victor Avalos, Xiaoyu Nie, Anbang Yang, Canming He, Sunil Kumar, and Kai Dieckmann. Field-programmable-gate-array-based digital frequency stabilization of low-phase-noise diode lasers. *Review of Scientific Instruments*, 94(6):063001, June 2023.

[24] W. F. McGrew, X. Zhang, R. J. Fasano, S. A. Schäffer, K. Beloy, D. Nicolodi, R. C. Brown, N. Hinkley, G. Milani, M. Schioppo, T. H. Yoon, and A. D. Ludlow. Atomic clock performance enabling geodesy below the centimetre level. *Nature*, 564(7734):87–90, December 2018.

[25] Yintao Ma, Zhixia Qiao, Yao Chen, Guoxi Luo, Mingzhi Yu, Yanbin Wang, Dejiang Lu, Libo Zhao, Ping Yang, Qijing Lin, and Zhuangde Jiang. In-situ determination of spin polarization in a single-beam fiber-coupled spin-exchange-relaxation-free atomic magnetometer with differential detection. *Opt. Express*, 31(3):3743–3754, January 2023.

[26] N. Kostylev, E. Ivanov, M. E. Tobar, and J. J. McFerran. Sub-doppler cooling of ytterbium with the $^1s_0 - {}^1p_1$ transition including $^{171}\,Yb$ (I=1/2). *J. Opt. Soc. Am. B*, 31(7):1614–1620, Jul 2014.

[27] Limeng Luo, Hao Qiao, Di Ai, Min Zhou, Shuang Zhang, Sheng Zhang, Changyue Sun, Qichao Qi, Chengquan Peng, Taoyun Jin, Wei Fang, Zhiqiang Yang, Tianchu Li, Kun Liang, and Xinye Xu. Absolute frequency measurement of an yb optical clock at the 10^{-16} level using international atomic time. *Metrologia*, 57(6):065017, October 2020.

[28] Esa Jaatinen, David J Hopper, and Julian Back. Residual amplitude modulation mechanisms in modulation transfer spectroscopy that use electro-optic modulators. *Measurement Science and Technology*, 20(2):025302, February 2009.

[29] Hui Shen, Liufeng Li, Jin Bi, Jia Wang, and Lisheng Chen. Systematic and quantitative analysis of residual amplitude modulation in Pound-Drever-Hall frequency stabilization. *Physical Review A*, 92(6):063809, December 2015.

[30] Chen-Fei Wu, Xue-Shu Yan, Li-Xun Wei, Pei Ma, Jian-Hui Tu, Jian-Wei Zhang, and Li-Jun Wang. Modulation transfer spectroscopy based on acousto-optic modulator with zero frequency shift. 27(11):114203.

[31] Geol Moon and Heung-Ryoul Noh. Linewidth in saturated absorption spectroscopy for two-level atoms: an empirical formula. *Appl. Opt.*, 57(14):3881–3883, May 2018.

[32] Heung-Ryoul Noh. Susceptibility for doppler-broadened two-level atoms in pump-probe spectroscopy: Analytical solutions revisited. *Journal of the Optical Society of America B*, 33:308, 03 2016.

[33] Danna Shen, Liangyu Ding, Qiuxin Zhang, Chenhao Zhu, Yuxin Wang, Wei Zhang, and Xiang Zhang. High-performance frequency stabilization of ultraviolet diode lasers by using dichroic atomic vapor spectroscopy and transfer cavity. *Chinese Physics B*, 29(7):074210, jun 2020.